Quantifying the effect of overland flow on Escherichia coli pulses during floods: use of a tracer-based approach in an erosion-prone tropical catchment

Laurie Boithias, Olivier Ribolzi, Guillaume Lacombe, Chanthamousone Thammahacksa, Norbert Silvera, Keooudone Latsachack, Bounsamay Soulileuth, Marion Viguier, Yves Auda, Elodie Robert, et al.

Quantifying the effect of overland flow on *Escherichia coli* pulses during floods: use of a tracer-based approach in an erosion-prone tropical catchment

Laurie BOITHIAS[1,*], Olivier RIBOLZI[1], Guillaume LACOMBE[2], Chanthamousone THAMMAHACKSA[3], Norbert SILVERA[4], Keooudone LATSACHACK[3], Bounsamay SOULILEUTH[3], Marion VIGUIER[3], Yves AUDA[1], Elodie ROBERT[1], Olivier EVRARD[5], Sylvain HUON[4], Thomas POMMIER[6], Cyril ZOUITEN[1], Oloth SENGTAHEUANGHOUNG[7], Emma ROCHELLE-NEWALL[4]

[1] Géosciences Environnement Toulouse, Université de Toulouse, CNES, CNRS, IRD, UPS, France

[2] CIRAD, UMR G-EAU, F-34398 Montpellier, France
G-EAU, Univ Montpellier, AgroParisTech, CIRAD, INRAE, Institut Agro, IRD, Montpellier, France

[3] IRD, Department of Agricultural Land Management (DALaM), P.O. Box 4199, Ban Nogviengkham, Xaythany District, Vientiane, Lao PDR

[4] Institute of Ecology and Environmental Sciences of Paris (iEES-Paris), Sorbonne Université, Univ Paris Est Creteil, IRD, CNRS, INRA, 4 place Jussieu, 75005 Paris, France

[5] Laboratoire des Sciences du Climat et de l'Environnement (LSCE/IPSL), Unité Mixte de Recherche 8212 (CEA/CNRS/UVSQ), Université Paris-Saclay, Gif-sur-Yvette, France

[6] Laboratoire d'Ecologie Microbienne, UMR1418 INRA, UMR 5557 CNRS, UCBL, VetAgroSup, Université de Lyon, Villeurbanne, France

[7] Department of Agricultural Land Management (DALaM), P.O. Box 4195, Ban Nogviengkham, Xaythany District, Vientiane, Lao PDR

* Corresponding author: laurie.boithias@get.omp.eu

Abstract

Bacterial pathogens in surface waters threaten human health. The health risk is especially high in developing countries where sanitation systems are often lacking or deficient. Considering twelve flash-flood events sampled from 2011 to 2015 at the outlet of a 60-ha tropical montane headwater catchment in Northern Lao PDR, and using *Escherichia coli* as a fecal indicator bacteria, our objective was to quantify the contributions of both surface runoff and sub-surface flow to the in-stream concentration of *E. coli* during flood events, by (1) investigating *E. coli* dynamics during flood events and among flood events and (2) designing and comparing simple statistical and mixing models to predict *E. coli* concentration in stream flow during flood events. We found that in-stream *E. coli* concentration is high regardless of the contributions of both surface runoff and sub-surface flow to the flood event. However, we measured the highest concentration of *E. coli* during the flood events that are predominantly driven by surface runoff. This indicates that surface runoff, and causatively soil surface erosion, are the primary drivers of in-stream *E. coli* contamination. This was further confirmed by the step-wise regression applied to instantaneous *E. coli* concentration measured in individual water samples collected during the flood events, and by the three models applied to each flood event (linear model, partial least square model, and mixing model). The three models showed that the percentage of surface runoff in stream flow was the best predictor of the flood event mean *E. coli* concentration. The mixing model yielded a Nash-Sutcliffe efficiency of 0.65 and showed that on average, 89% of the in-stream concentration of *E. coli* resulted from surface runoff, while the overall contribution of surface runoff to the stream flow was 41%. We also showed that stream flow turbidity and *E. coli* concentration were positively correlated, but that turbidity was not a strong predictor of *E. coli* concentration during flood events. These findings will help building adequate catchment-scale models to predict *E. coli* fate and transport, and mapping the related risk of fecal contamination in a global changing context.

Keywords

Surface runoff; Fecal Indicator Bacteria; Storm flow; Land-use change; Surface-sub surface flow separation; northern uplands of Lao PDR

Graphical abstract

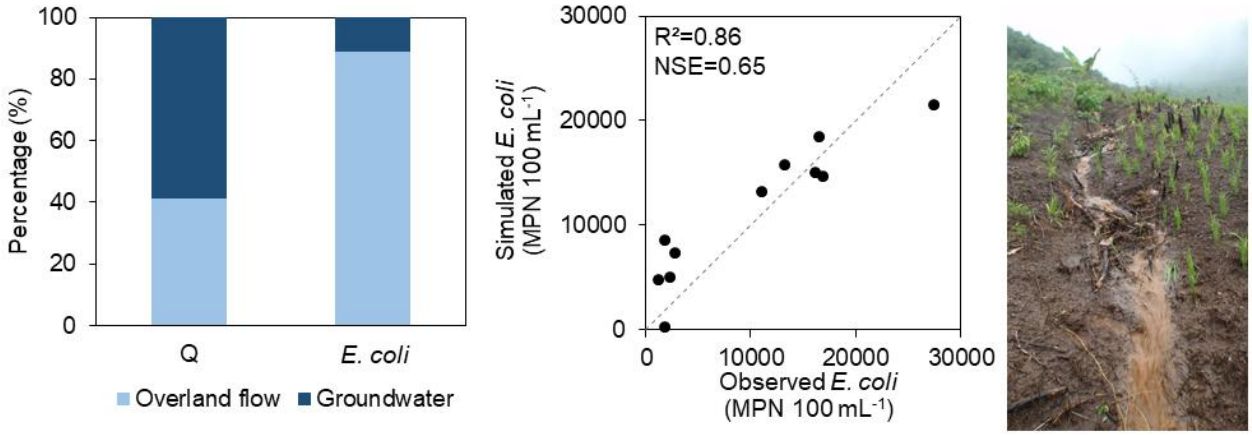

1. Introduction

The presence of bacterial pathogens in surface waters threatens human health. Pathogenic bacteria are etiological agents of several waterborne diseases such as diarrhea, which is globally a leading cause of death among all ages (1.31 million deaths in 2015) (Troeger et al., 2017). These bacterial pathogens can be of fecal origin, e.g. from cattle or from human feces where open defecation is practiced or where sanitation systems are lacking or deficient (Exley et al., 2015; Tong et al., 2016). In developing countries, untreated surface water is often used for drinking, cooking, bathing and washing, thus exposing the population to a high health risk (Boithias et al., 2016).

Catchment microbial response depends on complex interactions between spatial patterns of land use, soil types, antecedent conditions of soil, and rainfall characteristics (Kim et al., 2018; McKergow and Davies-Colley, 2010; Pachepsky et al., 2018; Strauch et al., 2014). In the tropics, the presence in stream water of Fecal Indicator Bacteria (FIB), such as *Escherichia coli* (*E. coli*), is known to be partly driven by surface runoff (Causse et al., 2015; Ribolzi et al., 2016a) and groundwater flow (Chuah and Ziegler, 2018). However, the underlying mechanisms of FIB dynamics during storms remain to be fully documented. For example, there is a need to better quantify the respective contributions of surface and sub-surface flows to stream flow (e.g. using geochemical tracers) to understand and model the transfers of *E. coli* at the catchment scale during a flood event (Cho et al., 2016; Kim et al., 2017) and to predict the relative contributions of surface and sub-surface flows to the overall in-stream *E. coli* contamination (Chin, 2011).

E. coli is known to be transported in water as free cells or cells attached to particles of soil, manure or sediment (Garcia-Armisen and Servais, 2009; Krometis et al., 2007; Soupir et al., 2010). While stream flow turbidity is often higher in tropical areas, as compared to temperate areas, suspended sediments are known to carry *E. coli* (Nguyen et al., 2016). However, the relationships between stream flow turbidity, suspended sediments concentration, and *E. coli* concentration, and their possible hysteretic patterns during flood events, have not been yet fully explored.

Several studies in the tropics have investigated the relationships between suspended sediments concentration and turbidity in rivers and lakes (Martinez et al., 2009; Robert et al., 2017, 2016; Ziegler et al., 2014), and few studies investigated the relationships between suspended sediments concentration and *E. coli* concentration (Boithias et al., 2016; Nguyen et al., 2016). However, to our knowledge, no study has yet investigated the relationships between turbidity and *E. coli* concentration. Given that in-stream *E. coli* concentration can vary rapidly during a flood event, a high-frequency sampling is required to characterize this variability. The latter is both time consuming and expensive. Therefore, a proxy-based approach is required and there is a need to verify if stream flow turbidity can be used as a proxy of *E. coli* concentration during flood events.

In rural Southeast Asia, such as the uplands of Northern Lao PDR, livestock grazing and the lack of adequate sanitation systems result in high levels of fecal contamination in surface waters during both high and low flow seasons (Boithias et al., 2016; Nguyen et al., 2016; Rochelle-Newall et al., 2016). In addition, Northern Lao PDR, like other mountainous regions in South-East Asia, is experiencing rapid changes in land use (Ribolzi et al., 2017; Turkelboom et al., 2008). Annual crops are replaced by tree plantations (e.g. teak) with limited understorey and litter coverage. This land-use change decreases soil water infiltration and increases surface runoff and soil erosion (Lacombe et al., 2018; Ribolzi et al., 2017; Song et al., 2020; Ziegler et al., 2004), but its impact on bacteria export has not yet been investigated.

Considering twelve flash-flood events sampled from 2011 to 2015 at the outlet of a 60-ha montane tropical headwater catchment in Northern Lao PDR, our objective was thus to quantify the contributions of both surface runoff and sub-surface flow to the in-stream concentration of *E. coli* during flood events, by (1) investigating *E. coli* dynamics during flood events and among flood events and (2) designing and comparing simple statistical and mixing models to predict *E. coli* concentration in stream flow during flood events.

2. Materials and methods

2.1. Study design

In this paper, we quantify the relative roles of both surface runoff and sub-surface flow in the contamination of stream water by *E. coli* in a tropical montane catchment. To do so, we measured fine temporal-scale discharge and stream flow electrical conductivity to calculate the relative contributions of surface runoff and sub-surface flow to total stream flow. For twelve flash-flood events from 2011 to 2015 (named with the letters A to L), we then investigated statistical relationships between surface runoff, sub-surface flow, *E. coli* concentration, together with turbidity, total suspended sediments concentration, land-use features (areal percentage of land cover and *E. coli* input), and flood event-integrated variables, i.e. total rainfall, maximum rainfall intensity, rainfall duration, soil antecedent conditions, peak discharge, total volume of stream water exported during the flood event, and flow coefficient. For each flood event, we applied a mixing model to calculate the relative contributions of surface runoff and of sub-surface flow to the overall in-stream contamination by *E. coli*, by assigning to each one of these two flow components a characteristic bacteria concentration based on *E. coli* measurements in overland flow (overland flow *E. coli* end-member) and in groundwater (groundwater *E. coli* end-member).

2.2. Study area: the Houay Pano catchment

The 0.6 km^2 Houay Pano headwater catchment is located 10 km south of Luang Prabang city in Northern Lao PDR (Fig. 1a), within the 800 000 km^2 Mekong basin. This experimental site (Boithias et al., 2020) is part of the critical zone observatories' network named Multiscale TROPIcal CatchmentS (M-TROPICS), which belongs to the French Research Infrastructure OZCAR (Gaillardet et al., 2018). This catchment can be considered as being representative of the montane agro-ecosystems of South-East Asia. The climate is sub-tropical humid and is characterized by a monsoon regime with a dry season from November to May, and a wet season from June to October. The mean annual (2001-2019) temperature is 23.4 °C while the

mean annual rainfall is 1 366 mm (CV=0.23), about 71 % (CV=0.09) of which falls during the wet season. Altitude within the catchment is 435-716 m (Fig. 1b) and the slope gradient is 1-135 % (mean=52 %). The Laksip village, located downstream the S4 station (Fig. 1b), includes 484 inhabitants (Census of 2015).

2.3. Land use and land-use change

Detailed land-cover surveys and mapping were conducted each year from 2011 to 2015 within the catchment (Boithias et al., 2020). The annual areal percentages of fallow (Fallow), teak trees (Teak), annual crops (Annual crop), and annual crops grown under young teak trees (Teak+Crop) were calculated using QGIS 2.6. We assessed the monthly *E. coli* input from 2011 to 2015 within the catchment with the monthly counting of human and domestic animal (swine and poultry) traffic within the catchment, with the daily feces production of humans and domestic animals, and with the *E. coli* content in their feces (Causse et al., 2015).

2.4. Rainfall measurements

Rainfall was measured by an automatic weather station (Campbell BWS200 equipped with ARG100, 0.2 mm capacity tipping-bucket) located within the catchment (Fig. 1b). Data was recorded at 6-min time interval from 2011 to 2012, and at 1-min time interval from 2013 to 2015. Data from 2013 to 2015 was then cumulated into a 6-min time series for consistency with the 2011-2012 sub-period.

2.5. Flow rate measurements and water quality monitoring

We measured stream water level at the S4 gauging station of the catchment outlet (Fig. 1b) within a V-notch weir equipped with a water level recorder (OTT Thalimedes) connected to a data logger, with 1-mm vertical precision at a minimum of 3-min time interval. To relate water level to discharge, a control rating curve was determined using both the velocity area method and the salt dilution method by slug injection. Samples of stream water were collected at S4 gauging station in clean, plastic bottles using an

automatic sampler (Automatic Pumping Type Sediment Sampler, ICRISAT) for the measurement of Total Suspended Sediments concentration ([TSS]), turbidity (Turbidity), Electrical Conductivity at 25°C (EC), and *E. coli* concentration ([*E. coli*]). The automatic sampler was triggered by the water level recorder to collect water after every 2-cm water level change during flood rising and every 5-cm water level change during flood recession.

[TSS] was measured in each sample after filtration on 0.2 µm porosity cellulose acetate filters (Sartorius) and evaporation at 105 °C for 48 h. Turbidity was determined with a turbidity meter (EUTECH Instruments TN-100) and EC with a conductivity meter (WTW340).

For nine flood events (events A, B, F-L), we measured [*E. coli*] with the standardized microplate method (ISO 9308-3). A water sub-sample was incubated at four dilution rates (i.e. 1:2, 1:20, 1:200 and 1:2000) in a 96-well microplate (MUG/EC, BIOKAR DIAGNOSTICS) for 48 h at 44 °C. Ringers' Lactate solution was used for the dilutions and one plate was used per sample. The number of positive wells for each microplate was noted and the Most Probable Number (MPN) per 100 mL was determined using the Poisson distribution. For three flood events (events C-E), we measured [*E. coli*] following the membrane-filter method (EPA Method 1603). A small quantity of each water sample was filtered through the filter membrane, which retained the bacterial cells. After filtration, this membrane was placed on a selective medium (Sartorius NKS Endo nutrient pads), and incubated at 44 °C for 24 h. Shiny green *E. coli* colonies were directly counted and expressed as Colony Forming Units (CFU) per 100 mL. Although "colony forming unit" techniques and "most probable number" techniques are known to give highly correlated results (e.g. Cho et al., 2010; Lušić et al., 2016; Wohlsen et al., 2006), we previously ensured that the two methods were consistent in the Houay Pano catchment conditions (unpublished work).

In addition, we monitored surface runoff in the different land uses of the catchment from 2011 to 2015 using 1-m² microplots (Patin et al., 2018). We annually installed between 6 and 29 microplots to collect

surface runoff water samples during each rainfall event and to measure EC with WTW340. In 2012 and 2014, we used sub-samples of surface runoff water to measure *E. coli* concentration in surface runoff as described previously. We calculated the mean concentration of *E. coli* in surface runoff by weighing the *E. coli* concentration exported from each land use by the annual areal percentage of each land use ([*E. coli*]$_{OF\text{-}TOT}$). We also measured the *E. coli* concentration in water samples taken from three piezometers (Ribolzi et al., 2018) and calculated the mean concentration of *E. coli* in groundwater ([*E. coli*]$_{GW\text{-}TOT}$).

2.6. Electrical conductivity-based hydrograph separation

We used a tracer-based approach to separate storm hydrographs into 'event water' and 'pre-event water'. This approach relies on a simple mixing model with two end-members and EC as a tracer. It is of relatively low cost compared to e.g. isotopic tracers and was successfully tested in the study catchment (Ribolzi et al., 2018). Based on previous field observations and measurements performed in the same study catchment (Patin et al., 2012; Ribolzi et al., 2011; Vigiak et al., 2008), the two end-members of the model (i.e. overland flow EC end-member in event water, and groundwater EC end-member in pre-event water) can be interpreted in terms of hydrological processes. Event water mainly includes infiltration excess that produces overland flow along hillslopes. Pre-event water relates to groundwater that feeds the stream during the storm event, plus the water in the stream channel prior to the storm event, which is also related to groundwater outflows. As suggested by Collins and Neal (1998), we verified the linearity between EC and the concentration of a conservative tracer to control the relevance of the EC-based approach in our context (Ribolzi et al., 2018). The mixing model applied to individual samples is described by the following equations:

$$Q = Q_{OF} + Q_{GW} \quad \text{Eq. 1}$$

$$Q \times EC = Q_{OF} \times EC_{OF} + Q_{GW} \times EC_{GW} \quad \text{Eq. 2}$$

where Q is the instantaneous stream water discharge at the catchment outlet (L s^{-1}), Q_{OF} is the instantaneous discharge of overland flow, i.e., event water or surface runoff (L s^{-1}), Q_{GW} is the

196 instantaneous discharge of groundwater, i.e., pre-event water or sub-surface flow (L s^{-1}), EC is the
197 instantaneous electrical conductivity measured in the stream (µS cm^{-1}), EC_{OF} is the electrical conductivity
198 in overland flow (overland flow EC end-member; µS cm^{-1}), approximated from electrical conductivity
199 measurements in samples of overland flow collected at the soil surface on hillslopes draining to the
200 stream, and EC_{GW} is the electrical conductivity in groundwater (groundwater EC end-member; µS cm^{-1}),
201 approximated from the stream electrical conductivity at the beginning of the flood event, since
202 groundwater is the only supply of water to the stream during inter-storm flow periods (Ribolzi et al.,
203 2005). For each individual sample, we calculated the relative contributions of Q_{OF} and of Q_{GW} to Q based
204 on Eq. 2, namely Q_{OF}% and of Q_{GW}% (in %).

205 We assessed the uncertainty in estimating the contributions of overland flow and groundwater flow to
206 the total stream flow using the formulation of Genereux (1998), which assigns an uncertainty specific to
207 each term in Eqs. 1 and 2. The accuracy of Q is considered to be within ±10% of the measured value,
208 while the uncertainty of EC is approximately ±5% (Ribolzi et al., 2018). The uncertainties of both EC_{OF} and
209 EC_{GW} are estimated from the coefficients of variation (CV) of overland flow and groundwater samples,
210 respectively.

211 ## 2.7. Flood-event variables

212 For each flood event, the mean concentration of *E. coli* ($[E.\ coli]_{mean}$) is equivalent to the average of the
213 instantaneous *E. coli* concentrations ([*E. coli*]) measured during the event, weighted by the
214 corresponding measurements of instantaneous discharge. We considered 13 candidate explanatory
215 variables to predict $[E.\ coli]_{mean}$:

216 - Rainfall duration (R_D, in min), total rainfall (R_{TOT}, in mm), maximum rainfall intensity (RI_{MAX}, in mm
217 h^{-1});

- Antecedent Precipitation Index (API, in mm), as a proxy of soil moisture conditions, calculated as $API_n = (API_{n-1} + P_{n-1}) \times e^{-\alpha \times t}$ where API_{n-1} is the antecedent precipitation index prior to rain event n-1 (mm), P_{n-1} is the rainfall precipitated during rain event n-1 (mm), α is the calibration coefficient usually set at 0.5 (day^{-1}), and t is the duration between P_n and P_{n-1} (day) (Descroix et al., 2002);
- Peak discharge during flood event (Q_{MAX}, in L s^{-1}), total volume of stream water during flood event (Q_{TOT}, in m^3), total volume of surface runoff, i.e. overland flow, during flood event (Q_{OF-TOT}, in m^3) and its contribution to Q_{TOT} (Q_{OF-TOT}%, in %), and volume of sub-surface flow during flood event (Q_{GW-TOT}, in m^3) and its contribution to Q_{TOT} (Q_{GW-TOT}%, in %);
- Flow coefficient of the flood event (K_E, no dimension), calculated as the ratio between Q_{TOT} and R_{TOT};
- Flood-event mean concentration of total suspended sediments concentration ($[TSS]_{mean}$, in g L^{-1}), calculated by weighting [TSS] by the discharge, and flood-event mean turbidity ($Turbidity_{mean}$, in NTU), calculated by weighting Turbidity by time.

2.8. Hysteresis

Combined with EC-based hydrograph separation, the analysis of rotational direction, curvature, and trend of hysteresis relationships can be used to interpret the relative contributions from surface water and groundwater, and analyte sources (Holz, 2010; Long et al., 2017). Here, we analyzed hysteresis patterns of EC, Turbidity, [TSS] and [*E. coli*] against discharge; [TSS], Turbidity and [*E. coli*] against Q_{OF}; Turbidity and [*E. coli*] against [TSS]; and [*E. coli*] against Turbidity. For each flood, we considered straight relationships when the p-value of the Pearson correlation was below 0.001. The threshold was voluntarily chosen very demanding to distinguish straight relationships from other hysteretic patterns.

2.9. Statistical analysis

We calculated correlations and regressions to identify explanatory variables predicting [*E. coli*] and [*E. coli*]$_{mean}$. Statistics were calculated with R statistical package version 3.4.3 (correlations), Minitab 18.1 (stepwise regression), and XLSTAT 20.1.1 (partial least square regression). An explanatory variable was considered to be statistically significantly different from zero when its p-value, derived from Student's t-test, was lower than 0.05.

2.9.1. Modelling instantaneous *E. coli* concentration [*E. coli*]

We first calculated Pearson correlations between [*E. coli*] and the eight hydrological variables measured or calculated for each sample (EC, Q, Q_{OF}, Q_{GW}, Q_{OF}%, Q_{GW}%, [TSS], and Turbidity). In addition, to select the best set of explanatory variables predicting [*E. coli*], we derived linear regressions from the 'step-wise regression' selection algorithm. This selection intended to maximize the prediction R^2 (R^2_{pred}) calculated by leave-one-out cross-validations. This performance criterion reflects the ability of the model to predict observations that were not used in the model calibration. Its maximization leads to greater parsimony in the number of explanatory variables (Helsel and Hirsch, 2002). We verified the required homoscedasticity of the model's residuals by visual inspection. Multi-collinearity among the selected explanatory variables was avoided by ensuring that the Variance Inflation Factor (VIF) never exceeded the value of 8 (Helsel and Hirsch, 2002). We didn't mix instantaneous measurements with flood-event variables or with variables assessed annually (Annual crop, Teak+Crop, Teak, and Fallow) or monthly (*E. coli* input).

2.9.2. Modelling mean concentration of *E. coli* per flood event [*E. coli*]$_{mean}$

We first calculated Pearson correlations between [*E. coli*]$_{mean}$ and the thirteen hydro-meteorological variables measured or calculated for each flood event (Table 1) and the five land-use related variables (Annual crop, Teak+Crop, Teak, Fallow, and *E. coli* input). In addition, we used Partial Least Square (PLS)

263 regression to detect dependencies between variables. PLS is able to handle datasets with a number of
264 variables higher than the number of observations. It is also poorly sensitive to multi-collinearity, and
265 handles missing data by imputation. The importance of each projected variable is estimated by the
266 Variable Importance in the Projection (VIP). We discarded the variables for which VIP values were below
267 1 (Ribolzi et al., 2016b; Wold, 1995).

268 ## 2.10. Mixing model of flood-event mean concentration of *E. coli*

269 We applied a simple mixing model with two end-members to predict $[E.\ coli]_{mean}$ and to separate the
270 contributions of both 'event water' and 'pre-event water' to the in-stream *E. coli* concentrations. Here
271 the two end-members of the model are *E. coli* concentration in event water (overland flow *E. coli* end-
272 member or $[E.\ coli]_{OF\text{-}TOT}$) and *E. coli* concentration in pre-event water (groundwater *E. coli* end-member
273 or $[E.\ coli]_{GW\text{-}TOT}$). The mixing model applied to flood-event mean variables is described by the following
274 equations:

$$Q_{TOT} = Q_{OF-TOT} + Q_{GW-TOT} \quad \text{Eq. 3}$$

$$Q_{TOT} \times [E.coli]_{mean} = Q_{OF-TOT} \times [E.coli]_{OF-TOT} + Q_{GW-TOT} \times [E.coli]_{GW-TOT} \quad \text{Eq. 4}$$

275 where Q_{TOT} is the total volume of stream water during flood event (m^3), $Q_{OF\text{-}TOT}$ is the total volume of
276 surface runoff, or overland flow, during flood event (m^3), $Q_{GW\text{-}TOT}$ is the total volume of sub-surface flow,
277 or groundwater flow, during flood event (m^3), $[E.\ coli]_{mean}$ is the flood-event mean concentration of *E. coli*
278 (MPN 100 mL^{-1}), $[E.\ coli]_{OF\text{-}TOT}$ is the mean concentration of *E. coli* exported in overland flow (MPN 100
279 mL^{-1}), calculated from *E. coli* concentration measured in samples of overland flow collected at the soil
280 surface on hillslopes draining to the stream, and $[E.\ coli]_{GW\text{-}TOT}$ is the mean concentration of *E. coli* in
281 groundwater (MPN 100 mL^{-1}), calculated from *E. coli* concentration measured in groundwater. This
282 approach was shown to yield a comparable or even higher performance when predicting in-stream
283 pathogen concentrations compared with more complex fate and transport models (Chin, 2011). We
284 applied the mixing model to the twelve flood events and compared its performance with the

285 performance of the PLS model. For each flood event, we calculated the relative contributions of [*E.*

286 *coli*]$_{OF\text{-}TOT}$ and of [*E. coli*]$_{GW\text{-}TOT}$ to [*E. coli*]$_{mean}$ based on Eq. 4, namely [*E. coli*]$_{OF\text{-}TOT}$% and of [*E. coli*]$_{GW\text{-}TOT}$%

287 (in %).

3. Results

3.1. *E. coli* dynamics during flood events and among flood events

The areal percentage of land use evolved from 2011 to 2015 (Fig. SI1): annual crop decreased from 28% to 4% of the catchment area, and teak and annual crop decreased from 12% to 0%, while teak increased from 18% to 36%, and fallow increased from 29% to 46%. Areal percentage of forest was constant at 8%. The *E. coli* input into the catchment decreased from a monthly average of $2x10^{15}$ in 2011 to a monthly average of $3x10^{14}$ in 2015 (Fig. SI2). Over the 2011-2015 period, the cumulated *E. coli* input for swine and poultry accounted for 0.01-0.38 % of the total *E. coli* input.

In the meantime, a total of 294 discharge peaks were recorded between January 1, 2011, and December 31, 2015 (Fig. 2), in response to a range of rainfall events (Fig. SI3, see interquartile ranges): 50 % of R_{TOT} ranged between 7 and 22 mm, 50 % of RI_{MAX} ranged between 24 and 60 mm h^{-1}, and 50 % of R_D ranged between 49 and 235 min. Q ranged from 0 to 1 807.6 L s^{-1} (30 L s^{-1} ha^{-1}), with a mean Q of 33.3 L s^{-1}.

We monitored twelve flood events (A to L) for stream water quality. Datasets for each of the twelve flood events are complete except EC measurements lacking for event A and Turbidity measurements lacking for event G, due to measurement devices' breakdown. A total of 99 stream water samples was collected: [TSS] ranged from 0.02 to 25.7 g L^{-1} while Turbidity ranged from 191.8 to 13 480 NTU (Fig. 3). *E. coli* were detected in all samples and [*E. coli*] ranged between 160 and 74 000 MPN 100 mL^{-1} (Fig. 3).

For the twelve flood events, rainfall was followed by an increase of Q, Turbidity, [TSS] and [*E. coli*] (Fig. 3). However, the peaks of Q, Turbidity, [TSS] and [*E. coli*] were often asynchronous (full description is given in the supplementary information). Hysteresis loops showed complex patterns mixing straight lines, simple clockwise or anti-clockwise loops, figures-of-eight or multiple hysteresis loops (summary is presented in Table SI1, full description is given in the supplementary information, including Figs. SI4-SI7).

The uncertainty bands enclosing Q_{OF} and Q_{GW} in Fig. 3 show that the hydrograph could be clearly separated for each flood event. Flood event C was the only event where the stream flow was virtually 100% groundwater flow. Excluding flood event C, $Q_{OF\text{-}TOT}$% ranged between 17 and 80% (Fig. 4a). The average $Q_{OF\text{-}TOT}$% was 41% (CV=0.59).

The twelve flood events corresponded to a range of storm characteristics in terms of R_{TOT}, RI_{MAX} and R_D (Fig. SI3, Fig. 2). Q_{MAX} ranged from 31.7 to 967.9 L s^{-1} (Table 1, Fig. 3). Three flood events occurred after dry periods (events B, G, and I: API<10), whereas others occurred shortly after a previous flood event (events D, E, and J: API>30) or later (events A, C, F, H, K, and L: 10<API<20) (Table 1). $[E.\ coli]_{mean}$ ranged from 1 125 and 27 375 MPN 100 mL^{-1}.

Mean EC_{OF} was 55 µS cm^{-1} (CV=0.7) over the 2011-2015 period (65 surface runoff water samples). Mean EC_{GW} was 256 µS cm^{-1} (CV=0.42) among the twelve flood events. $[E.\ coli]_{OF\text{-}TOT}$ was 24 880, 27 292, 27 441, 26 987, and 26 935 MPN 100 mL^{-1} in 2011, 2012, 2013, 2014, and 2015, respectively (26 surface runoff water samples). $[E.\ coli]_{GW\text{-}TOT}$ was 277 MPN 100 mL^{-1} (6 groundwater samples).

3.2. Statistical analysis

3.2.1. Modelling instantaneous *E. coli* concentration [*E. coli*]

Considering all water samples collected during the flood events (Fig. SI8), [*E. coli*] was positively correlated to Q (r=0.54, p<0.001), Q_{OF} (r=0.56, p<0.001), Q_{OF}% (r=0.51, p<0.001), [TSS] (r=0.43, p<0.001), and Turbidity (r=0.43, p<0.001), and was negatively correlated to EC (r=-0.31, p=0.003), and to Q_{GW}% (r=-0.51, p<0.001). Turbidity was positively correlated to [TSS] (r=0.82, p<0.001).

From the stepwise regression, [*E. coli*] was best predicted by [TSS] and Q_{OF} (Eq. 5):

$$[E.coli] = 4995 + 689 \cdot [TSS] + 41.49 \cdot Q \quad \text{Eq. 5}$$

T-values and p-values of the coefficients are given in Table SI2. The R^2 of the model is 35.3 % and the R^2_{pred} is 24.42 %.

3.2.2. Modelling mean concentration of *E. coli* per flood event $[E.\ coli]_{mean}$

$[E.\ coli]_{mean}$ was positively correlated to Q_{MAX} (r=0.71, p=0.009), Q_{TOT} (r=0.59, p=0.042), $Q_{OF\text{-}TOT}$ (r=0.72, p=0.012), and $Q_{OF\text{-}TOT}$% (r=0.93, p<0.001), and was negatively correlated to $Q_{GW\text{-}TOT}$% (r=-0.93, p<0.001) (Fig. SI9).

From the above, we found that $Q_{OF\text{-}TOT}$% was the variable the most positively correlated to $[E.\ coli]_{mean}$. The linear model is:

$$[E.coli]_{mean} = 332 \cdot Q_{OF-TOT}\% - 3\,749 \qquad \text{Eq. 6}$$

The R^2 between predicted and observed $[E.\ coli]_{mean}$ was 0.87 while the Nash-Sutcliffe efficiency (NSE) was 0.84 (Fig. 5a). Excluding event C that was driven by groundwater flow only (and for which the linear model predicted a negative value), $[E.\ coli]_{mean}$ predicted by the linear model ranged from 1 981 to 22 825 MPN 100 mL^{-1}.

These latter trends are confirmed by the PLS regression (Fig. 6a), which shows that Axis 1 mostly explains the variables $Q_{OF\text{-}TOT}$% (r=0.863), $Q_{GW\text{-}TOT}$% (r=-0.863), Q_{MAX} (r= 0.859), and $Q_{OF\text{-}TOT}$ (r=0.815) whereas Axis 2 mostly explains the variable RI_{MAX} (r=0.563). Hence, Axis 1 corresponds to variables that are strongly related to stream water whereas Axis 2 corresponds to variables describing rainfall and soil moisture conditions. Accordingly, the twelve flood events were scattered along the two axes, with the flood events of highest $[E.\ coli]_{mean}$ in the right panel (Fig. 6b). The variables with VIP values above 1 were $Q_{OF\text{-}TOT}$%, $Q_{GW\text{-}TOT}$%, Q_{MAX}, $Q_{OF\text{-}TOT}$, and Q_{TOT} when considering one component and $Q_{OF\text{-}TOT}$%, $Q_{GW\text{-}TOT}$%, $[TSS]_{mean}$, Q_{MAX}, and $Q_{OF\text{-}TOT}$ when considering two components (Fig. 6c; Table SI3). The statistical model given by the PLS is given in Table SI3. The R^2 between predicted and observed $[E.\ coli]_{mean}$ was 0.83 while the NSE was 0.78 (Fig. 5b). Excluding event C that was driven by groundwater flow only (and for which

the PLS model predicted a negative value), $[E.\ coli]_{mean}$ predicted by the PLS model ranged from 1 067 to 23 237 MPN 100 mL^{-1}.

$[E.\ coli]_{mean}$ predicted by the mixing model ranged from 277 to 21 572 MPN 100 mL^{-1}. The R^2 between predicted and observed $[E.\ coli]_{mean}$ was 0.86 while the NSE was 0.65 (Fig. 5c). Flood event C was the only event where the percentage of *E. coli* was 100% from groundwater flow. Excluding flood event C, $[E.\ coli]_{OF\text{-}TOT}$% ranged from 95 to virtually 100% (Fig. 4b). The average $[E.\ coli]_{OF\text{-}TOT}$% was 89% (CV=0.33).

4. Discussion

4.1. High *E. coli* concentration pulses match high overland flow pulses

The analysis of the twelve monitored flood events (Table 1) shows that $[E.\ coli]_{mean}$ was high regardless of the flood event characteristics: $[E.\ coli]_{mean}$ ranged between 1 125 and 27 375 MPN 100 mL^{-1}. The order of magnitude of the maximum [*E. coli*] is about 10^5 MPN 100 mL^{-1}. All these values exceed the 1 000 MPN 100 mL^{-1} threshold provided by e.g. the European Directive 2006/7/EC for bathing water quality.

Although rainfall is known to reactivate hydrological connectivity (Bracken et al., 2013), rainfall characteristics such as R_{T0T}, RI_{MAX}, and R_D, did not appear as strong explanatory variables of $[E.\ coli]_{mean}$ (Fig. 6 and Fig. SI9). Variations in [*E. coli*] and $[E.\ coli]_{mean}$ between flood events may be explained by rainfall spatial distribution and the timing between rainfall events: the rainfall distribution will determine which areas draining animal and human manure are activated, whereas the timing between events may indicate which catchment microbial stocks have accumulated to high levels (McKergow and Davies-Colley, 2010). In Houay Pano catchment, variations in concentration between flood events may also be explained by *E. coli* input distribution at the soil surface, as the land use is mixed (Fig. SI1). Indeed, based on this twelve-event dataset and hysteresis analysis, we could not find any clear, consistent trend at the outlet of the Houay Pano catchment (Table SI1) and we thus could not identify any primary bacteria source.

The land use change in Houay Pano catchment was rapid and led to the simultaneous increase of teak tree plantations and of fallow areas (Ribolzi et al., 2017). Previous plot- and catchment-scale results showed higher surface runoff and suspended matter export when teak tree plantations increased (Lacombe et al., 2018; Mügler et al., 2019; Ribolzi et al., 2017; Song et al., 2020), suggesting that higher numbers of *E. coli* could be transferred to the river. However, land use characteristics such as land use variables (Annual crop, Teak+Crop, Teak, Fallow, and *E. coli* input) did not appear as strong explanatory

383 variables of [*E. coli*]$_{mean}$ (Fig. 6 and Fig. SI10). Growing teak trees and fallow requires less people in the
384 field compared to annual crops. Since field workers practice open defecation, less workers imply lower
385 input of *E. coli* into the catchment. The contribution of domestic animals to the overall *E. coli* input being
386 only 0.01-0.38 % of the total *E. coli* input, the consequence of the extension of teak tree plantation and
387 of fallow in Houay Pano from 2011 to 2015 (Fig. SI1) is the overall decrease of the *E. coli* input into the
388 catchment over the same period (Fig. SI2).

389 The highest [*E. coli*]$_{mean}$ was often associated to flood events with highest Q_{MAX} (events J and L) and
390 dominant surface runoff ($Q_{OF\text{-}TOT}$%>50: events D, and I-L), confirming the role of surface runoff, and
391 subsequent soil surface erosion, in *E. coli* transfers to the stream (Causse et al., 2015) (Table 1, Fig. 6).
392 For flood events where sub-surface flow was dominating ($Q_{OF\text{-}TOT}$%<50: events B, C, and E-H), [*E. coli*]$_{mean}$
393 was in general lower, although exceeding 1 000 MPN 100 mL^{-1}. High *E. coli* concentrations even when
394 sub-surface flow was dominating suggest that streambanks and the streambed may release stored *E. coli*
395 (Chu et al., 2011; Park et al., 2017; Stocker et al., 2018) since sediment deposited at the bottom of the
396 stream may act as an *E. coli* reservoir (Pachepsky et al., 2017; Rochelle-Newall et al., 2015; Smith et al.,
397 2008). In fact, the concentration of *E. coli* in Houay Pano streambed sediment is about 40 000 MPN g^{-1}
398 (Ribolzi et al., 2016a), but we cannot exclude that *E. coli* is simultaneously transferred from the hillslope
399 with surface runoff, if hillslope soil surface is highly contaminated. We also found both clockwise and
400 anti-clockwise [*E. coli*]-[TSS] and [*E. coli*]-Turbidity hysteresis loops, and in some cases figure-of-eight
401 patterns (Table SI1, Fig. SI6 and Fig. SI7). This further suggests that the erosion of bacteria stores is not
402 strictly driven by soil erosion, but also by in-stream sediment resuspension (Evrard et al., 2016; Gourdin
403 et al., 2015; Huon et al., 2017). In parallel, possibly less *E. coli*-contaminated sub-surface flow, or return
404 flow, may dilute in the stream the *E. coli* concentration originating from surface runoff and thus mitigate
405 the in-stream microbial contamination.

4.2. Predictive models of *E. coli* concentration: performances and usefulness

To our knowledge, few studies have reported predictive models using independent variables to explain *E. coli* concentration and, to the best of our knowledge, they were all developed in temperate areas (Chen and Chang, 2014; Hathaway et al., 2010). The models suggested by Chen and Chang (2014) included antecedent precipitation, stream temperature, and TSS concentration, and gave an R^2 of 0.27-0.61 depending on the season and the catchment. The model suggested by Hathaway et al. (2010) included temperature, rainfall, and humidity, and had an R^2 of 0.7462. The variety of explanatory variables among models reflects the variety of driving processes driving *E. coli* fate and transport among catchments.

4.2.1. Modelling instantaneous *E. coli* concentration [*E. coli*]

[*E. coli*] was equally correlated to both [TSS] and Turbidity ($r=0.43$, $p<0.001$; Fig. SI8) while Turbidity was correlated with [TSS] ($r=0.82$, $p<0.001$, Fig. SI8). The strong correlation between Turbidity and [TSS] is in line with the results obtained in other studies in tropical areas, such as Ziegler et al. (2014) for rivers in Thailand and Robert et al. (2017) in West African lakes and ponds. The relationships between [TSS] and [*E. coli*] and between Turbidity and [*E. coli*] are qualified by hysteretic trends (Figs. SI6 and SI7, respectively) during flood events. Notably, little hysteresis is observed between [TSS] and Turbidity (Fig. SI6). Hysteretic trends may illustrate the uncertainty when predicting *E. coli* by a proxy such as turbidity: sources of sediments may not exactly coincide with sources of *E. coli*. For example, these relationships may not apply in large mixed-land use catchments, because of the multiple, geographically separated, *E. coli* and turbidity sources. This may limit the usefulness of using turbidity as a proxy of *E. coli* near the catchment outlet (McKergow and Davies-Colley, 2010). Another explanation of the hysteresis is the nature and the properties of the suspended sediments, that may change during the flood event: bacteria may be less prone to attach to sand-rich suspended particles (Oliver et al., 2007). Similarly, hysteresis in Turbidity-[TSS] relationships may be explained by changing reflectance properties of the suspended

sediments depending on particle size, shape, mineralogy, aggregation/flocculation, dissolved light-absorbing matter and bubbles, because of the spatial heterogeneity of rainfall and suspended sediment sources at the catchment scale (Navratil et al., 2011; Ziegler et al., 2014). A last uncertainty source in the relationships between [*E. coli*], [TSS], and Turbidity, is the possible exhaustion of the *E. coli* stock within the catchment after a succession of flood events.

From the step-wise regression analysis, the predictive model for [*E. coli*] includes [TSS] and Q_{OF} as explanatory variables (Eq. 5). The two explanatory variables reflect the two processes driving *E. coli* transport within the catchment: Q_{OF} reflects the mobilization of *E. coli* with relative contributions of surface and sub-surface flows along the flood event, whereas [TSS] reflects the attachment of *E. coli* to soil particles and/or streambed resuspended sediments (Garcia-Armisen and Servais, 2009; Nguyen et al., 2016). Overall, higher *E. coli* concentration is related to higher surface runoff and higher suspended matter in the stream flow. The value of the intercept term in Eq. 5 corresponds to *E. coli* concentration during base flow (Boithias et al., 2016; Kim et al., 2018), i.e. when [TSS] and Q_{OF} tend to zero because there is no surface runoff during inter-storm periods, in other words when groundwater is the only supply to stream flow and EC tends to EC_{GW}.

The two variables best predicting [*E. coli*], namely [TSS] and Q_{OF}, can be assessed with proxies. [TSS] could be interchanged with Turbidity, since [TSS] and Turbidity are correlated, as discussed above. Similarly, EC appears strongly related to Q_{OF} (and Q) by a hyperbolic function (Fig. SI8). Using EC as a proxy of Q has already been proposed in Alpine headwaters (Cano-Paoli et al., 2019). Both of these proxies can be monitored *in situ* at high frequencies.

4.2.2. Modelling mean concentration of *E. coli* per flood event $[E.\ coli]_{mean}$

The PLS regression analysis (Table SI3) confirmed the analysis of the correlation matrix (Fig. SI9): $Q_{OF\text{-}TOT}$% and $Q_{GW\text{-}TOT}$% were the best predictors of $[E.\ coli]_{mean}$ (r= 0.93 and -0.93, respectively). Land uses that

453 favor higher $Q_{OF\text{-}TOT}$% or lower $Q_{GW\text{-}TOT}$%, such as erosion-prone teak trees plantations (Lacombe et al.,
454 2016; Ribolzi et al., 2017), or more intense rainfall events, will lead to higher in-stream concentrations of
455 *E. coli* (Fig. 6a and Fig. SI10) and thus higher fecal contamination risk. Hence, a model based on $Q_{OF\text{-}TOT}$%
456 or $Q_{GW\text{-}TOT}$% appears relevant to predict $[E.\ coli]_{mean}$. Such a basic tool may help local and national
457 stakeholders to assess the fecal contamination risk by testing global change scenarios in target
458 catchments.

459 In this study, the mixing model of $[E.\ coli]_{mean}$ based on $Q_{OF\text{-}TOT}$% and $Q_{GW\text{-}TOT}$% had a R^2 of 0.86 and a NSE
460 of 0.65. The NSE value is lower than the NSE values' range reported by Chin (2011) in six nested
461 catchments in Georgia, United-States. However, in our study the values of both overland flow and
462 groundwater end-members were measured in the field, conversely to Chin (2011) who numerically
463 optimized the values of the two end-members. The performance of the mixing model is lower in terms of
464 NSE than those of the PLS and the linear models (NSE = 0.78 and 0.84, respectively). However, the PLS
465 model is difficult to implement because of the large number of variables it implies, and both the linear
466 and the PLS models are constrained by their validity domains.

467 Within a catchment, the sources of *E. coli* are the *E. coli* transferred from hillslopes with surface runoff,
468 as discussed in section 4.1, and the resuspension from the streambed, whereas the sinks of *E. coli* are the
469 deposition of the bacterium on the streambed and its decay in the water column. Since rainfall events in
470 the Houay Pano catchment last 0.5-5 hours, considering a decay rate of 0.3-0.6 d^{-1} (Nguyen et al., 2016),
471 the removal of *E. coli* in the water column from bacteria population decay is negligible during a flood
472 event. Since the mixing model is able to accurately predict the flood-event mean concentration of *E. coli*
473 at the catchment outlet, the deposition of *E. coli* on the streambed is either negligible or compensated
474 by the resuspension. The percentage of *E. coli* resuspended from streambed during a flood is about 11%
475 (Ribolzi et al., 2016a), which implies that the compensated *E. coli* deposition, e.g. in small wetlands along
476 the main stream, is about 11% as well. Finally, since the possible sources and sinks of *E. coli* are negligible

compared to the bacterium transport processes during flood events, the approximation of the simple model that only considers two end-members, namely the *E. coli* concentration in both surface runoff and groundwater, is acceptable.

Hence, we could calculate the relative contributions of surface runoff and of sub-surface flow to the in-stream *E. coli* contamination. Excluding flood event C that was driven by groundwater flow, more than 95% of $[E.\ coli]_{mean}$ resulted from overland flow, even for flood events where the percentage of overland flow was small (<20%, events E and G). The average contribution of overland flow to the flood-event mean concentration of *E. coli* was 89%, while the average contribution of overland flow to the flood-event mean stream flow was 41% (Fig. 4). In other words, the contribution of groundwater to the in-stream *E. coli* contamination was low during flood events, even though the contribution of groundwater to stream water flow was greater than that of overland flow, i.e. when base flow index (BFI) was over 0.5. In comparison, with similar BFI values, Chin (2011) reported bacteria loads from surface runoff in the range of 80–90%, with the remainder mostly originating from base flow, and negligible background loads from the catchment.

5. Conclusion

To our knowledge, few papers have reported the statistical relationships between *E. coli* and its environmental drivers (meteorological, hydrological, and land use variables) and the present study is the first one to investigate *E. coli* dynamics during flood events in a tropical humid catchment. We conclude that:

- Regardless of the contribution of sub-surface flow to the flood, in-stream *E. coli* concentration is high, suggesting that the streambed *E. coli* store is high. However, highest concentrations of *E. coli* are measured for the flood events that are driven by surface runoff, suggesting that surface runoff, and consequently soil erosion, are the primary drivers of in-stream *E. coli* contamination;
- The three predictive models (linear model, partial least square model, and mixing model) show that the percentage of surface runoff in stream flow is the best predictor of the flood event mean concentration of *E. coli*;
- A simple mixing model based on the relative contributions of both overland flow and groundwater, and on the *E. coli* concentration in both overland flow and groundwater, is reliable to predict in-stream flood-event mean *E. coli* concentration (NSE=0.65). On average, 89% of the in-stream concentration of *E. coli* is supplied by surface runoff, while the overall contribution of surface runoff to the stream flow is 41%.
- Stream flow turbidity and *E. coli* concentration are positively correlated, but turbidity is not a strong predictor of *E. coli* concentration during flood events;

Predictive models based on turbidity and electrical conductivity may be used to provide real-time estimates of in-stream *E. coli* concentration, whereas a mixing model may provide flood-event mean information. Such simple models may help to assess the impact of global change on in-stream *E. coli* contamination. They could thus be used to assess the risk of water borne diseases such as diarrhea, in rural areas where mammals, including humans, practice open defecation, and to design early warning

systems. Applied over long periods of time, the models might be used to calculate *E. coli* input-output load balances. Such basic modelling studies would thus help to assess the long-term impact of land-use change on the microbial quality of surface water.

Future work is required to better understand the pathways of FIB at catchment scale. For example, there is a need to characterize the interactions between ground and surface waters, and the role of the hyporheic zone, as sources of contaminant. Furthermore, the partition between free and particle-attached *E. coli* should be quantified to better understand and predict the probability that bacteria is deposited on the streambed during the flood recession stage and re-suspended in the water column during the next flood rising stage. These findings are of primary importance to build adequate catchment-scale models to accurately simulate *E. coli* fate and transport, and thus better assess fecal contamination risk in a global changing context.

Acknowledgments

The authors sincerely thank the Lao Department of Agricultural Land Management (DALaM) for its support, including granting the permission for field access, and the M-TROPICS Critical Zone Observatory (https://mtropics.obs-mip.fr/), which belongs to the French Research Infrastructure OZCAR (http://www.ozcar-ri.org/), for data access. This study was funded by the GIS-Climat (http://www.gisclimat.fr/projet/pastek.html) and by the French National Research Agency (TecItEasy project; ANR-13-AGRO-0007). LB thanks the Research Institute for Development (IRD) for her postdoctoral grant 2016-2017 (*Accueil de post-doctorants / Campagne 2015*; www.ird.fr).

References

Boithias, L., Auda, Y., Audry, S., et al., 2020. Dataset from the Multiscale TROPIcal CatchmentS critical zone observatory M-TROPICS II: land use, hydrology and sediment production monitoring in Houay Pano, northern Lao PDR. Hydrol. Process. Submitted.

Boithias, L., Choisy, M., Souliyaseng, N., Jourdren, M., Quet, F., Buisson, Y., Thammahacksa, C., Silvera, N., Latsachack, K., Sengtaheuanghoung, O., Pierret, A., Rochelle-Newall, E., Becerra, S., Ribolzi, O., 2016. Hydrological regime and water shortage as drivers of the seasonal incidence of diarrheal diseases in a tropical montane environment. PLoS Negl. Trop. Dis. 10, e0005195. https://doi.org/10.1371/journal.pntd.0005195

Bracken, L.J., Wainwright, J., Ali, G.A., Tetzlaff, D., Smith, M.W., Reaney, S.M., Roy, A.G., 2013. Concepts of hydrological connectivity: Research approaches, pathways and future agendas. Earth-Sci. Rev. 119, 17–34. https://doi.org/10.1016/j.earscirev.2013.02.001

Cano-Paoli, K., Chiogna, G., Bellin, A., 2019. Convenient use of electrical conductivity measurements to investigate hydrological processes in Alpine headwaters. Sci. Total Environ. 685, 37–49. https://doi.org/10.1016/j.scitotenv.2019.05.166

Causse, J., Billen, G., Garnier, J., Henri-des-Tureaux, T., Olasa, X., Thammahacksa, C., Latsachak, K.O., Soulileuth, B., Sengtaheuanghoung, O., Rochelle-Newall, E., Ribolzi, O., 2015. Field and modelling studies of Escherichia coli loads in tropical streams of montane agro-ecosystems. J. Hydro-Environ. Res. 9, 496–507. https://doi.org/10.1016/j.jher.2015.03.003

Chen, H.J., Chang, H., 2014. Response of discharge, TSS, and E. coli to rainfall events in urban, suburban, and rural watersheds. Env. Sci Process. Impacts 16, 2313–2324. https://doi.org/10.1039/C4EM00327F

Chin, D.A., 2011. Quantifying pathogen sources in streams by hydrograph separation. J. Environ. Eng. 137, 770–781.

Cho, K.H., Han, D., Park, Y., Lee, S.W., Cha, S.M., Kang, J.-H., Kim, J.H., 2010. Evaluation of the relationship between two different methods for enumeration fecal indicator bacteria: Colony-forming unit and most probable number. J. Environ. Sci. 22, 846–850. https://doi.org/10.1016/S1001-0742(09)60187-X

Cho, K.H., Pachepsky, Y.A., Oliver, D.M., Muirhead, R.W., Park, Y., Quilliam, R.S., Shelton, D.R., 2016. Modeling fate and transport of fecally-derived microorganisms at the watershed scale: State of the science and future opportunities. Water Res. 100, 38–56. https://doi.org/10.1016/j.watres.2016.04.064

Chu, Y., Salles, C., Tournoud, M.-G., Got, P., Troussellier, M., Rodier, C., Caro, A., 2011. Faecal bacterial loads during flood events in Northwestern Mediterranean coastal rivers. J. Hydrol. 405, 501–511. https://doi.org/10.1016/j.jhydrol.2011.05.047

Chuah, C.J., Ziegler, A.D., 2018. Temporal Variability of Faecal Contamination from On-Site Sanitation Systems in the Groundwater of Northern Thailand. Environ. Manage. https://doi.org/10.1007/s00267-018-1016-7

Collins, R.U., Neal, C., 1998. The hydrochemical impacts of terraced agriculture, Nepal. Sci. Total Environ. 212. https://doi.org/10.1016/S0048-9697(97)00342-2

Descroix, L., Nouvelot, J.-F., Vauclin, M., 2002. Evaluation of an antecedent precipitation index to model runoff yield in the western Sierra Madre (North-west Mexico). J. Hydrol. 263, 114–130. https://doi.org/10.1016/S0022-1694(02)00047-1

Evrard, O., Laceby, J.P., Huon, S., Lefèvre, I., Sengtaheuanghoung, O., Ribolzi, O., 2016. Combining multiple fallout radionuclides (137Cs, 7Be, 210Pbxs) to investigate temporal sediment source dynamics in tropical, ephemeral riverine systems. J. Soils Sediments 16, 1130–1144. https://doi.org/10.1007/s11368-015-1316-y

585 Exley, J.L.R., Liseka, B., Cumming, O., Ensink, J.H.J., 2015. The Sanitation Ladder, What Constitutes an
586 Improved Form of Sanitation? Environ. Sci. Technol. 49, 1086–1094.
587 https://doi.org/10.1021/es503945x
588 Gaillardet, J., Braud, I., Hankard, F., Anquetin, S., Bour, O., Dorfliger, N., de Dreuzy, J.R., Galle, S., Galy, C.,
589 Gogo, S., Gourcy, L., Habets, F., Laggoun, F., Longuevergne, L., Le Borgne, T., Naaim-Bouvet, F.,
590 Nord, G., Simonneaux, V., Six, D., Tallec, T., Valentin, C., Abril, G., Allemand, P., Arènes, A., Arfib,
591 B., Arnaud, L., Arnaud, N., Arnaud, P., Audry, S., Comte, V.B., Batiot, C., Battais, A., Bellot, H.,
592 Bernard, E., Bertrand, C., Bessière, H., Binet, S., Bodin, J., Bodin, X., Boithias, L., Bouchez, J.,
593 Boudevillain, B., Moussa, I.B., Branger, F., Braun, J.J., Brunet, P., Caceres, B., Calmels, D.,
594 Cappelaere, B., Celle-Jeanton, H., Chabaux, F., Chalikakis, K., Champollion, C., Copard, Y., Cotel,
595 C., Davy, P., Deline, P., Delrieu, G., Demarty, J., Dessert, C., Dumont, M., Emblanch, C., Ezzahar, J.,
596 Estèves, M., Favier, V., Faucheux, M., Filizola, N., Flammarion, P., Floury, P., Fovet, O., Fournier,
597 M., Francez, A.J., Gandois, L., Gascuel, C., Gayer, E., Genthon, C., Gérard, M.F., Gilbert, D.,
598 Gouttevin, I., Grippa, M., Gruau, G., Jardani, A., Jeanneau, L., Join, J.L., Jourde, H., Karbou, F.,
599 Labat, D., Lagadeuc, Y., Lajeunesse, E., Lastennet, R., Lavado, W., Lawin, E., Lebel, T., Le
600 Bouteiller, C., Legout, C., Lejeune, Y., Le Meur, E., Le Moigne, N., Lions, J., Lucas, A., Malet, J.P.,
601 Marais-Sicre, C., Maréchal, J.C., Marlin, C., Martin, P., Martins, J., Martinez, J.M., Massei, N.,
602 Mauclerc, A., Mazzilli, N., Molénat, J., Moreira-Turcq, P., Mougin, E., Morin, S., Ngoupayou, J.N.,
603 Panthou, G., Peugeot, C., Picard, G., Pierret, M.C., Porel, G., Probst, A., Probst, J.L., Rabatel, A.,
604 Raclot, D., Ravanel, L., Rejiba, F., René, P., Ribolzi, O., Riotte, J., Rivière, A., Robain, H., Ruiz, L.,
605 Sanchez-Perez, J.M., Santini, W., Sauvage, S., Schoeneich, P., Seidel, J.L., Sekhar, M.,
606 Sengtaheuanghoung, O., Silvera, N., Steinmann, M., Soruco, A., Tallec, G., Thibert, E., Lao, D.V.,
607 Vincent, C., Viville, D., Wagnon, P., Zitouna, R., 2018. OZCAR: The French Network of Critical Zone
608 Observatories. Vadose Zone J. 17, 180067. https://doi.org/10.2136/vzj2018.04.0067
609 Garcia-Armisen, T., Servais, P., 2009. Partitioning and Fate of Particle-Associated E. coli in River Waters.
610 Water Environ. Res. 81, 21–28. https://doi.org/10.2175/106143008X304613
611 Genereux, D., 1998. Quantifying uncertainty in tracer-based hydrograph separations. Water Resour. Res.
612 34, 915–919. https://doi.org/10.1029/98WR00010
613 Gourdin, E., Huon, S., Evrard, O., Ribolzi, O., Bariac, T., Sengtaheuanghoung, O., Ayrault, S., 2015. Sources
614 and export of particle-borne organic matter during a monsoon flood in a catchment of northern
615 Laos. Biogeosciences 12, 1073–1089. https://doi.org/10.5194/bg-12-1073-2015
616 Hathaway, J.M., Hunt, W.F., Simmons, O.D., 2010. Statistical Evaluation of Factors Affecting Indicator
617 Bacteria in Urban Storm-Water Runoff. J. Environ. Eng. 136, 1360–1368.
618 https://doi.org/10.1061/(ASCE)EE.1943-7870.0000278
619 Helsel, D.R., Hirsch, R.M., 2002. Chapter A3: Statistical Methods in Water Resources, in: Techniques of
620 Water-Resources Investigations of the United States Geological Survey. Book 4, Hydrologic
621 Analysis and Interpretation.
622 Holz, G.K., 2010. Sources and processes of contaminant loss from an intensively grazed catchment
623 inferred from patterns in discharge and concentration of thirteen analytes using high intensity
624 sampling. J. Hydrol. 383, 194–208. https://doi.org/10.1016/j.jhydrol.2009.12.036
625 Huon, S., Evrard, O., Gourdin, E., Lefèvre, I., Bariac, T., Reyss, J.-L., Henry des Tureaux, T.,
626 Sengtaheuanghoung, O., Ayrault, S., Ribolzi, O., 2017. Suspended sediment source and
627 propagation during monsoon events across nested sub-catchments with contrasted land uses in
628 Laos. J. Hydrol. Reg. Stud. 9, 69–84. https://doi.org/10.1016/j.ejrh.2016.11.018
629 Kim, M., Boithias, L., Cho, K.H., Sengtaheuanghoung, O., Ribolzi, O., 2018. Modeling the Impact of Land
630 Use Change on Basin-scale Transfer of Fecal Indicator Bacteria: SWAT Model Performance. J.
631 Environ. Qual. 47, 1115–1122. https://doi.org/10.2134/jeq2017.11.0456

Kim, M., Boithias, L., Cho, K.H., Silvera, N., Thammahacksa, C., Latsachack, K., Rochelle-Newall, E., Sengtaheuanghoung, O., Pierret, A., Pachepsky, Y.A., Ribolzi, O., 2017. Hydrological modeling of Fecal Indicator Bacteria in a tropical mountain catchment. Water Res. 119, 102–113. https://doi.org/10.1016/j.watres.2017.04.038

Krometis, L.-A.H., Characklis, G.W., Simmons, O.D., Dilts, M.J., Likirdopulos, C.A., Sobsey, M.D., 2007. Intra-storm variability in microbial partitioning and microbial loading rates. Water Res. 41, 506–516. https://doi.org/10.1016/j.watres.2006.09.029

Lacombe, G., Ribolzi, O., de Rouw, A., Pierret, A., Latsachak, K., Silvera, N., Pham Dinh, R., Orange, D., Janeau, J.-L., Soulileuth, B., Robain, H., Taccoen, A., Sengphaathith, P., Mouche, E., Sengtaheuanghoung, O., Tran Duc, T., Valentin, C., 2016. Contradictory hydrological impacts of afforestation in the humid tropics evidenced by long-term field monitoring and simulation modelling. Hydrol. Earth Syst. Sci. 20, 2691–2704. https://doi.org/10.5194/hess-20-2691-2016

Lacombe, G., Valentin, C., Sounyafong, P., de Rouw, A., Soulileuth, B., Silvera, N., Pierret, A., Sengtaheuanghoung, O., Ribolzi, O., 2018. Linking crop structure, throughfall, soil surface conditions, runoff and soil detachment: 10 land uses analyzed in Northern Laos. Sci. Total Environ. 616–617, 1330–1338. https://doi.org/10.1016/j.scitotenv.2017.10.185

Long, D.T., Voice, T.C., Xagaroraki, I., Chen, A., Wu, H., Lee, E., Oun, A., Xing, F., 2017. Patterns of c-q hysteresis loops and within an integrative pollutograph for selected inorganic and organic solutes and E. coli in an urban salted watershed during winter-early spring periods. Appl. Geochem. 83, 93–107. https://doi.org/10.1016/j.apgeochem.2017.03.002

Lušić, D.V., Jozić, S., Cenov, A., Glad, M., Bulić, M., Lušić, D., 2016. Escherichia coli in marine water: Comparison of methods for the assessment of recreational bathing water samples. Mar. Pollut. Bull. 113, 438–443. https://doi.org/10.1016/j.marpolbul.2016.10.044

Martinez, J.M., Guyot, J.L., Filizola, N., Sondag, F., 2009. Increase in suspended sediment discharge of the Amazon River assessed by monitoring network and satellite data. Catena 79, 257–264. https://doi.org/10.1016/j.catena.2009.05.011

McKergow, L.A., Davies-Colley, R.J., 2010. Stormflow dynamics and loads of *Escherichia coli* in a large mixed land use catchment. Hydrol. Process. 24, 276–289. https://doi.org/10.1002/hyp.7480

Mügler, C., Ribolzi, O., Janeau, J.-L., Rochelle-Newall, E., Latsachack, K., Thammahacksa, C., Viguier, M., Jardé, E., Henri-Des-Tureaux, T., Sengtaheuanghoung, O., Valentin, C., 2019. Experimental and modelling evidence of short-term effect of raindrop impact on hydraulic conductivity and overland flow intensity. J. Hydrol. 570, 401–410. https://doi.org/10.1016/j.jhydrol.2018.12.046

Navratil, O., Esteves, M., Legout, C., Gratiot, N., Nemery, J., Willmore, S., Grangeon, T., 2011. Global uncertainty analysis of suspended sediment monitoring using turbidimeter in a small mountainous river catchment. J. Hydrol. 398, 246–259. https://doi.org/10.1016/j.jhydrol.2010.12.025

Nguyen, H.T.M., Le, Q.T.P., Garnier, J., Janeau, J.-L., Rochelle-Newall, E., 2016. Seasonal variability of faecal indicator bacteria numbers and die-off rates in the Red River basin, North Viet Nam. Sci. Rep. 6, 21644. https://doi.org/10.1038/srep21644

Oliver, D.M., Clegg, C.D., Heathwaite, A.L., Haygarth, P.M., 2007. Preferential Attachment of Escherichia coli to Different Particle Size Fractions of an Agricultural Grassland Soil. Water. Air. Soil Pollut. 185, 369–375. https://doi.org/10.1007/s11270-007-9451-8

Pachepsky, Y., Stocker, M., Saldaña, M.O., Shelton, D., 2017. Enrichment of stream water with fecal indicator organisms during baseflow periods. Environ. Monit. Assess. 189, 51. https://doi.org/10.1007/s10661-016-5763-8

Pachepsky, Y.A., Allende, A., Boithias, L., Cho, K., Jamieson, R., Hofstra, N., Molina, M., 2018. Microbial Water Quality: Monitoring and Modeling. J. Environ. Qual. 47, 931–938. https://doi.org/10.2134/jeq2018.07.0277

680 Park, Y., Pachepsky, Y., Hong, E.-M., Shelton, D., Coppock, C., 2017. Release from Streambed to Water
681 Column during Baseflow Periods: A Modeling Study. J. Environ. Qual. 46, 219–226.
682 https://doi.org/10.2134/jeq2016.03.0114
683 Patin, J., Mouche, E., Ribolzi, O., Chaplot, V., Sengtahevanghoung, O., Latsachak, K.O., Soulileuth, B.,
684 Valentin, C., 2012. Analysis of runoff production at the plot scale during a long-term survey of a
685 small agricultural catchment in Lao PDR. J. Hydrol. 426–427, 79–92.
686 https://doi.org/10.1016/j.jhydrol.2012.01.015
687 Patin, J., Mouche, E., Ribolzi, O., Sengtahevanghoung, O., Latsachak, K.O., Soulileuth, B., Chaplot, V.,
688 Valentin, C., 2018. Effect of land use on interrill erosion in a montane catchment of Northern
689 Laos: An analysis based on a pluri-annual runoff and soil loss database. J. Hydrol. 563, 480–494.
690 https://doi.org/10.1016/j.jhydrol.2018.05.044
691 Ribolzi, O., Evrard, O., Huon, S., de Rouw, A., Silvera, N., Latsachack, K.O., Soulileuth, B., Lefèvre, I.,
692 Pierret, A., Lacombe, G., Sengtaheuanghoung, O., Valentin, C., 2017. From shifting cultivation to
693 teak plantation: effect on overland flow and sediment yield in a montane tropical catchment. Sci.
694 Rep. 7, 3987. https://doi.org/10.1038/s41598-017-04385-2
695 Ribolzi, O., Evrard, O., Huon, S., Rochelle-Newall, E., Henri-des-Tureaux, T., Silvera, N., Thammahacksac,
696 C., Sengtaheuanghoung, O., 2016a. Use of fallout radionuclides (7Be, 210Pb) to estimate
697 resuspension of Escherichia coli from streambed sediments during floods in a tropical montane
698 catchment. Environ. Sci. Pollut. Res. 23, 3427–3435. https://doi.org/10.1007/s11356-015-5595-z
699 Ribolzi, O., Lacombe, G., Pierret, A., Robain, H., Sounyafong, P., de Rouw, A., Soulileuth, B., Mouche, E.,
700 Huon, S., Silvera, N., Latxachak, K.O., Sengtaheuanghoung, O., Valentin, C., 2018. Interacting land
701 use and soil surface dynamics control groundwater outflow in a montane catchment of the lower
702 Mekong basin. Agric. Ecosyst. Environ. 268, 90–102. https://doi.org/10.1016/j.agee.2018.09.005
703 Ribolzi, O., Patin, J., Bresson, L.M., Latsachack, K.O., Mouche, E., Sengtaheuanghoung, O., Silvera, N.,
704 Thiébaux, J.P., Valentin, C., 2011. Impact of slope gradient on soil surface features and
705 infiltration on steep slopes in northern Laos. Geomorphology 127, 53–63.
706 https://doi.org/10.1016/j.geomorph.2010.12.004
707 Ribolzi, O., Rochelle-Newall, E., Dittrich, S., Auda, Y., Newton, P.N., Rattanavong, S., Knappik, M.,
708 Soulileuth, B., Sengtaheuanghoung, O., Dance, D.A.B., Pierret, A., 2016b. Land use and soil type
709 determine the presence of the pathogen Burkholderia pseudomallei in tropical rivers. Environ.
710 Sci. Pollut. Res. 23, 7828–7839. https://doi.org/10.1007/s11356-015-5943-z
711 Ribolzi, O., Silvera, N., Xayyakummanh, K., Latchachak, K., Tasaketh, S., Vanethongkham, K., 2005. The
712 use of pH to spot groundwater inflows along the stream of a cultivated catchment in the
713 northern Lao PDR. Lao J. Agric. For. 10, 72–84.
714 Robert, E., Grippa, M., Kergoat, L., Pinet, S., Gal, L., Cochonneau, G., Martinez, J.-M., 2016. Monitoring
715 water turbidity and surface suspended sediment concentration of the Bagre Reservoir (Burkina
716 Faso) using MODIS and field reflectance data. Int. J. Appl. Earth Obs. Geoinformation 52, 243–
717 251. https://doi.org/10.1016/j.jag.2016.06.016
718 Robert, E., Kergoat, L., Soumaguel, N., Merlet, S., Martinez, J.-M., Diawara, M., Grippa, M., 2017. Analysis
719 of Suspended Particulate Matter and Its Drivers in Sahelian Ponds and Lakes by Remote Sensing
720 (Landsat and MODIS): Gourma Region, Mali. Remote Sens. 9, 1272.
721 https://doi.org/10.3390/rs9121272
722 Rochelle-Newall, E., Nguyen, T.M.H., Le, T.P.Q., Sengtaheuanghoung, O., Ribolzi, O., 2015. A short review
723 of fecal indicator bacteria in tropical aquatic ecosystems: knowledge gaps and future directions.
724 Front. Microbiol. 6, 308. https://doi.org/10.3389/fmicb.2015.00308
725 Rochelle-Newall, E.J., Ribolzi, O., Viguier, M., Thammahacksa, C., Silvera, N., Latsachack, K., Dinh, R.P.,
726 Naporn, P., Sy, H.T., Soulileuth, B., Hmaimum, N., Sisouvanh, P., Robain, H., Janeau, J.-L.,
727 Valentin, C., Boithias, L., Pierret, A., 2016. Effect of land use and hydrological processes on

728 Escherichia coli concentrations in streams of tropical, humid headwater catchments. Sci. Rep. 6,
729 32974. https://doi.org/10.1038/srep32974
730 Smith, J., Edwards, J., Hilger, H., Steck, T.R., 2008. Sediment can be a reservoir for coliform bacteria
731 released into streams. J. Gen. Appl. Microbiol. 54, 173–179.
732 https://doi.org/10.2323/jgam.54.173
733 Song, L., Boithias, L., Sengtaheuanghoung, O., Oeurng, C., Valentin, C., Souksavath, B., Sounyafong, P., de
734 Rouw, A., Soulileuth, B., Silvera, N., Lattanavongkot, B., Pierret, A., Ribolzi, O., 2020. Understory
735 Limits Surface Runoff and Soil Loss in Teak Tree Plantations of Northern Lao PDR. Water 12,
736 2327. https://doi.org/10.3390/w12092327
737 Soupir, M.L., Mostaghimi, S., Dillaha, T., 2010. Attachment of *Escherichia coli* and Enterococci to Particles
738 in Runoff. J. Environ. Qual. 39, 1019–1027. https://doi.org/10.2134/jeq2009.0296
739 Stocker, M.D., Penrose, M., Pachepsky, Y.A., 2018. Spatial Patterns of Concentrations in Sediment before
740 and after High-Flow Events in a First-Order Creek. J. Environ. Qual. 47, 958–966.
741 https://doi.org/10.2134/jeq2017.11.0451
742 Strauch, A.M., Mackenzie, R.A., Bruland, G.L., Tingley, R., Giardina, C.P., 2014. Climate Change and Land
743 Use Drivers of Fecal Bacteria in Tropical Hawaiian Rivers. J. Environ. Qual. 43, 1475–1483.
744 https://doi.org/10.2134/jeq2014.01.0025
745 Tong, Y., Yao, R., He, W., Zhou, F., Chen, C., Liu, X., Lu, Y., Zhang, W., Wang, X., Lin, Y., Zhou, M., 2016.
746 Impacts of sanitation upgrading to the decrease of fecal coliforms entering into the environment
747 in China. Environ. Res. 149, 57–65. https://doi.org/10.1016/j.envres.2016.05.009
748 Troeger, C., Forouzanfar, M., Rao, P.C., 65 other authors, 2017. Estimates of global, regional, and
749 national morbidity, mortality, and aetiologies of diarrhoeal diseases: a systematic analysis for the
750 Global Burden of Disease Study 2015. Lancet Infect. Dis. 17, 909–948.
751 https://doi.org/10.1016/S1473-3099(17)30276-1
752 Turkelboom, F., Poesen, J., Trébuil, G., 2008. The multiple land degradation effects caused by land-use
753 intensification in tropical steeplands: A catchment study from northern Thailand. Catena 75,
754 102–116. https://doi.org/10.1016/j.catena.2008.04.012
755 Vigiak, O., Ribolzi, O., Pierret, A., Sengtaheuanghoung, O., Valentin, C., 2008. Trapping Efficiencies of
756 Cultivated and Natural Riparian Vegetation of Northern Laos. J. Environ. Qual. 37, 889–897.
757 https://doi.org/10.2134/jeq2007.0251
758 Wohlsen, T., Bates, J., Vesey, G., Robinson, W.A., Katouli, M., 2006. Evaluation of the methods for
759 enumerating coliform bacteria from water samples using precise reference standards. Lett. Appl.
760 Microbiol. 42, 350–356. https://doi.org/10.1111/j.1472-765X.2006.01854.x
761 Wold, S., 1995. PLS for Multivariate Linear Modelling. In: van de Waterbeemd H. (ed.), QSAR:
762 Chemometric Methods in Molecular Design. Vol 2. Wiley-VCH, Weinheim, Germany. pp. 195–
763 218.
764 Ziegler, A.D., Benner, S.G., Tantasirin, C., Wood, S.H., Sutherland, R.A., Sidle, R.C., Jachowski, N., Nullet,
765 M.A., Xi, L.X., Snidvongs, A., Giambelluca, T.W., Fox, J.M., 2014. Turbidity-based sediment
766 monitoring in northern Thailand: Hysteresis, variability, and uncertainty. J. Hydrol. 519, 2020–
767 2039. https://doi.org/10.1016/j.jhydrol.2014.09.010
768 Ziegler, A.D., Giambelluca, T.W., Tran, L.T., Vana, T.T., Nullet, M.A., Fox, J., Vien, T.D., Pinthong, J.,
769 Maxwell, J.., Evett, S., 2004. Hydrological consequences of landscape fragmentation in
770 mountainous northern Vietnam: evidence of accelerated overland flow generation. J. Hydrol.
771 287, 124–146. https://doi.org/10.1016/j.jhydrol.2003.09.027
772

773

774 List of figures

775

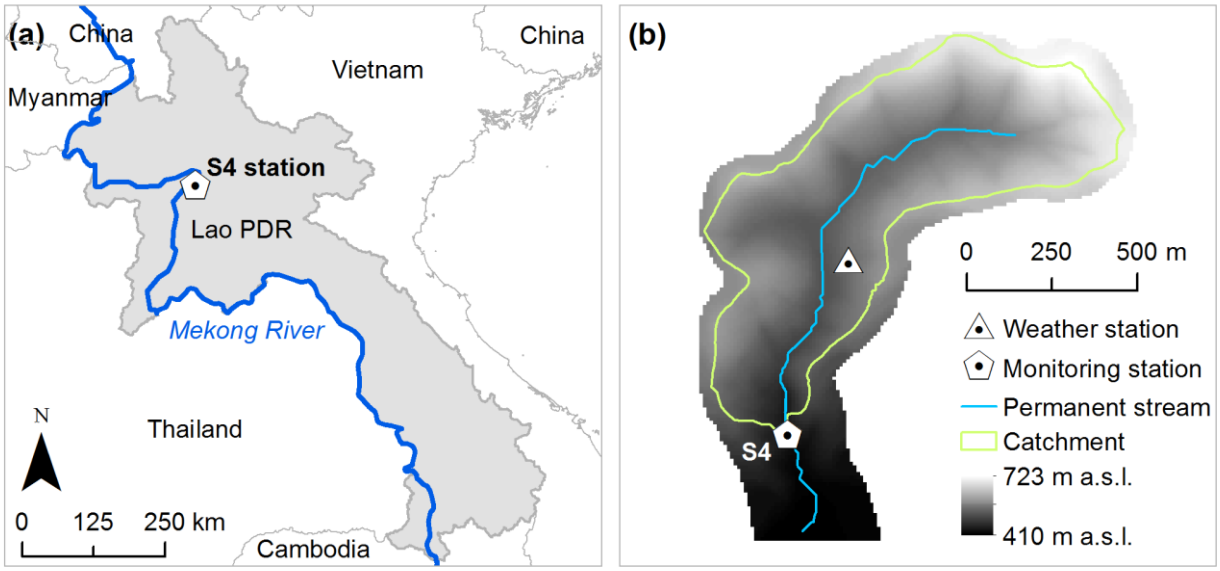

776

777 Fig. 1. (a) Location of the S4 outlet of the Houay Pano catchment in northern Lao PDR; (b) River gauging
778 and sampling station S4, weather station, and altitudes. Altitudes are given in meters above sea level (m
779 a.s.l.).

780

781

782

783

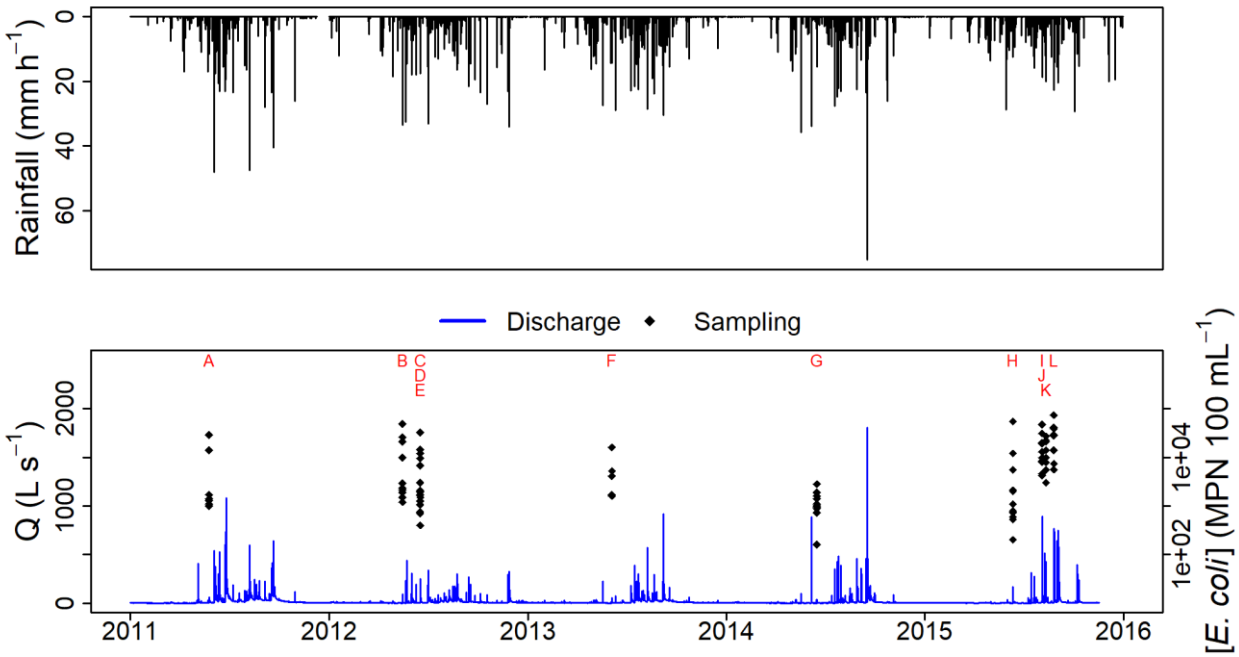

784

785 Fig. 2. Rainfall (mm h^{-1}) and discharge (Q, in L s^{-1}) for the 2011-2015 period, and *E. coli* concentration ([*E.*

786 *coli*], in MPN 100 mL^{-1}) for twelve flood events from 2011 to 2015 at the outlet of the Houay Pano

787 catchment, northern Lao PDR. The flood events of 16-17 June 2012 (C, D, and E) and of 4 August 2015 (I

788 and J) have been decomposed into 3 and 2 separate flood events. Details of these two flood events is

789 shown in Fig. 3. Although [*E. coli*] measures for events C-E were expressed in CFU 100 mL^{-1}, they are

790 reported as MPN 100 mL^{-1} for the sake of simplicity.

791

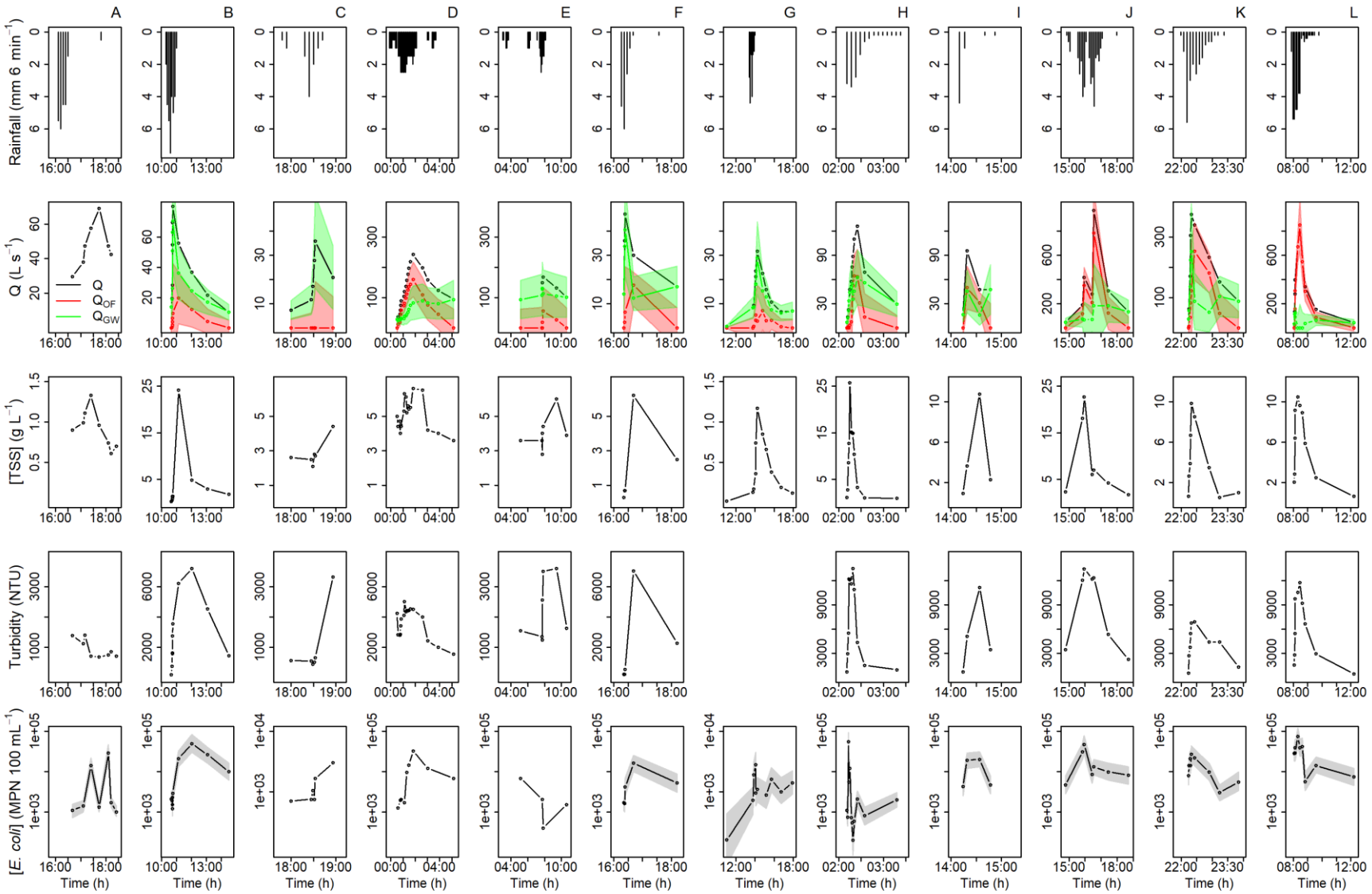
A
B
C
D
E
F
G
H
I
J
K
L
Rainfall (mm 6 min^{-1})
Q (L s^{-1})
Q
Q_{OF}
Q_{GW}
[TSS] (g L^{-1})
Turbidity (NTU)
[*E. coli*] (MPN 100 mL^{-1})
Time (h)

792

Fig. 3. Monitored flood events from 2011 to 2015 at the outlet of the Houay Pano catchment, northern Lao PDR. Rainfall: rainfall (mm); Q: discharge (L s^{-1}); Q_{OF}: surface runoff (L s^{-1}); Q_{GW}: sub-surface flow (L s^{-1}); [TSS]: total suspended sediments concentration (g L^{-1}); Turbidity: turbidity (NTU); [*E. coli*]: *E. coli* concentration (MPN 100 mL^{-1}). Measurements of turbidity were lacking for event G. Although [*E. coli*] measures for events C-E were expressed in CFU 100 mL^{-1}, they are reported as MPN 100 mL^{-1} for the sake of simplicity. Red and green bands for Q_{OF} and Q_{GW}, respectively, are uncertainty bands calculated with the Genereux (1998) method. Grey bands for [*E. coli*] are uncertainty intervals given by Poisson distribution when using the standardized microplate method.

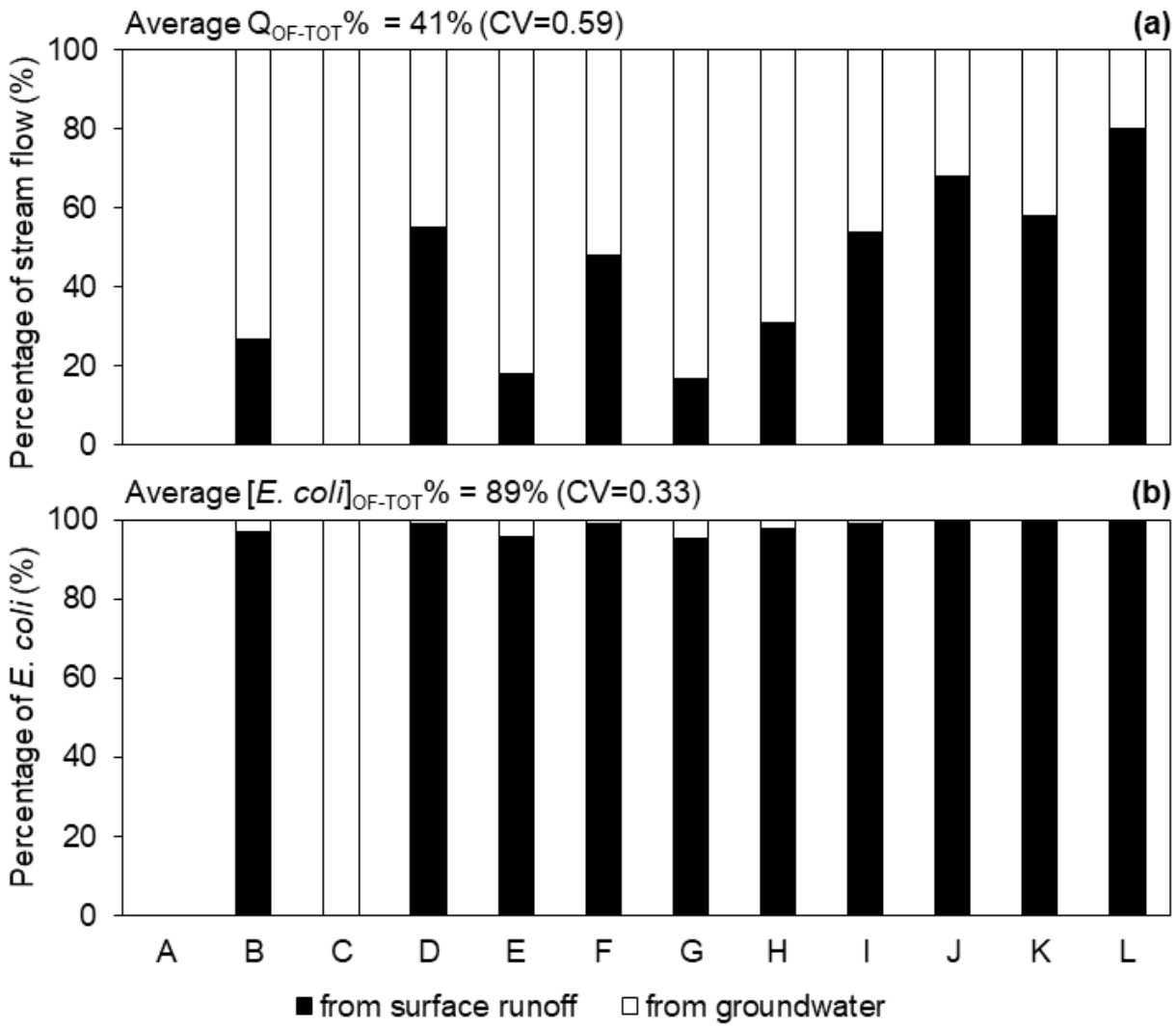

800

801 Fig. 4. Contributions (in %) of overland flow and of groundwater flow in (a) flood-event total volume of
802 stream flow, and in (b) flood-event total *E. coli* number. The twelve flood events were sampled from
803 2011 to 2015 at the outlet of the Houay Pano catchment, northern Lao PDR. Measurements of electrical
804 conductivity were missing for event A. Average Q_{OF-TOT}% and average [*E. coli*]$_{OF-TOT}$% are the average
805 contribution of overland flow to the in-stream flow and the average percentage of *E. coli* resulting from
806 overland flow, respectively. CV: coefficient of variation.

807

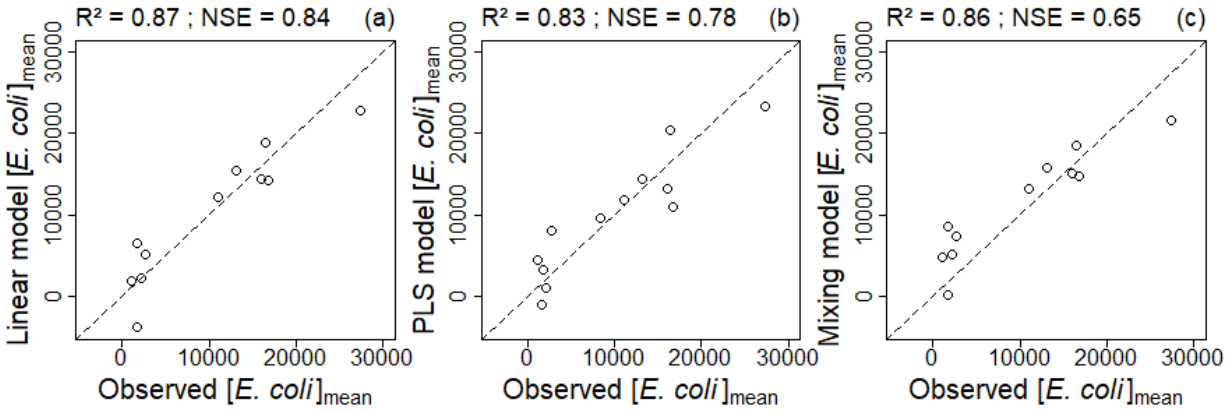

808

809 Fig. 5. Mean *E. coli* concentration per flood event ($[E.\ coli]_{mean}$): comparison of models' predictions with

810 observed values (MPN 100 mL^{-1}). (a) $Q_{OF\text{-}TOT}$%-based linear model against observed $[E.\ coli]_{mean}$; (b) PLS

811 model against observed $[E.\ coli]_{mean}$; (c) Mixing model against observed $[E.\ coli]_{mean}$. R^2: coefficient of

812 determination; NSE: Nash-Sutcliffe Efficiency. The twelve flood events were sampled from 2011 to 2015

813 at the outlet of the Houay Pano catchment, northern Lao PDR.

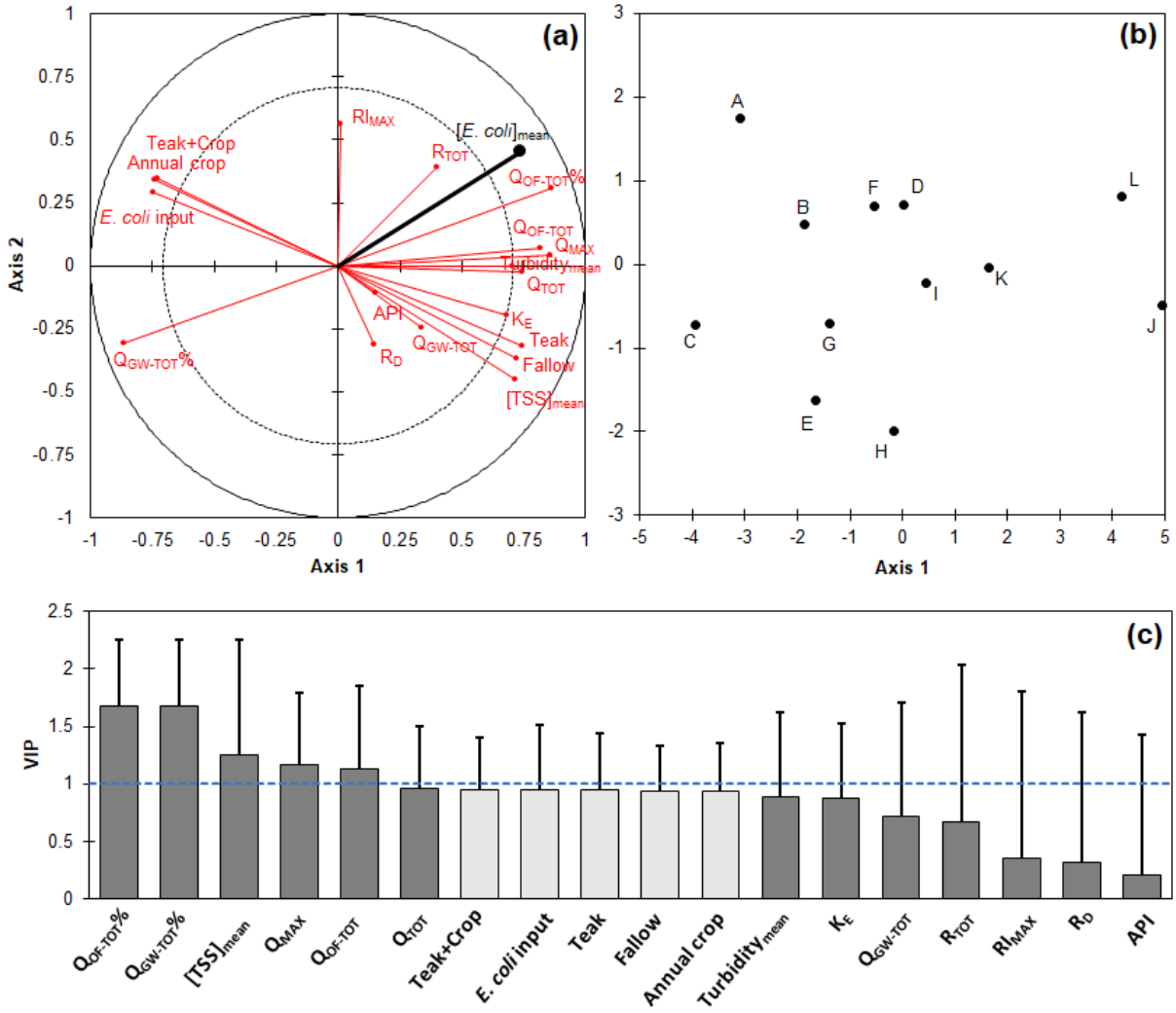

814

815 Fig. 6. Partial Least Square regression analysis where the flood-event mean concentration of *E. coli* ([*E.*

816 *coli*]$_{mean}$) is explained by hydro-meteorological and land-use variables: (a) *E. coli* located in the

817 correlations circle with 13 meteorological and hydrological variables and 5 land-use variables; (b) Map of

818 observations (twelve flood events from 2011 to 2015 at the outlet of the Houay Pano catchment,

819 northern Lao PDR); (c) Variable Importance in Projection (VIP) of the 18 variables for two components.

820 R_D: event rainfall duration; R_{TOT}: cumulated rainfall over the event; RI_{MAX}: maximum rainfall intensity; API:

821 antecedent precipitation index; Q_{MAX}: peak discharge during the event; Q_{TOT}: total volume of stream

822 water exported during the event; $Q_{OF\text{-}TOT}$: total volume of surface runoff exported during the event; $Q_{OF\text{-}TOT}$%: percentage of surface runoff during the event calculated as $Q_{OF\text{-}TOT}/Q_{TOT}*100$; $Q_{GW\text{-}TOT}$: total volume

of sub-surface flow exported during the event; $Q_{GW\text{-}TOT}$%: percentage of sub-surface flow during the event calculated as $Q_{GW\text{-}TOT}/Q_{TOT}*100$; K_E: flow coefficient calculated as Q_{TOT}/R_{TOT}; $[TSS]_{mean}$: flood-event mean total suspended sediments concentration; $Turbidity_{mean}$: flood-event mean turbidity; Fallow: annual percentage of the catchment area covered by fallow; Teak: annual percentage of the catchment area covered by teak trees; Annual crop: annual percentage of the catchment area covered by annual crops; Teak+Crop: annual percentage of the catchment area covered by annual crops grown under young teak trees; *E. coli* input: monthly *E. coli* input within the catchment.

List of tables

Table 1. Hydro-meteorological characteristics of the selected flood events from 2011 to 2015 at the outlet of the Houay Pano catchment, northern Lao PDR.

	Rainfall					Discharge					Water quality			
Event	**Start date Time**	**R_D (min)**	**R_{TOT} (mm)**	**RI_{MAX} (mm h^{-1})**	**API (mm)**	**Q_{MAX} (L s^{-1})**	**Q_{TOT} (m^3)**	**Q_{OF-TOT} (m^3)**	**Q_{OF-TOT}% (%)**	**K_E (%)**	**n (-)**	**$[TSS]_{mean}$ (g L^{-1})**	**$Turbidity_{mean}$ (NTU)**	**$[E.\ coli]_{mean}$ (MPN 100 mL^{-1})**
A	05/25/2011 16:06	24	22.5	60	15.5	69.1	305.5			2.3	8	1.0	993.6	8388
B	05/15/2012 10:18	42	33.5	75	2.8	80.3	553.4	146.7	27	2.7	10	4.9	5466.0	2672
C	06/16/2012 17:48	54	10.5	40	15.0	35.8	69.7	0.0	0	1.1	6	2.9	594.2	1682
D	06/17/2012 00:00	228	39	25	48.6	242.0	2620.8	1432.4	55	11.2	18	5.3	3252.9	16053
E	06/17/2012 03:00	306	19	25	40.6	168.4	2471.3	440.9	18	21.6	7	4.1	2578.0	2181
F	06/04/2013 16:11	82	14.6	60	12.3	47.0	215.6	103.3	48	2.5	5	2.0	5860.3	11020
G	06/16/2014 13:19	36	15.4	44	9.3	31.7	222.6	38.4	17	2.4	11	0.6		1125
H	06/12/2015 02:06	74	13.2	34	11.1	125.8	308.9	96.4	31	4.0	12	10.1	3696.0	1748
I	08/04/2015 13:22	50	6	44	4.3	95.2	127.4	69.1	54	3.8	4	4.8	6809.8	16776
J	08/04/2015 14:49	131	34.6	46	30.9	967.9	5554.2	3796.0	68	26.7	7	9.8	7790.9	16403
K	08/11/2015 21:59	81	20.8	56	17.4	374.7	1378.9	804.9	58	11.0	9	6.0	5205.8	13112
L	08/26/2015 07:48	116	32.4	54	16.2	849.6	3903.6	3118.3	80	20.0	10	8.2	4822.8	27375

R_D: duration of rainfall event; R_{TOT}: cumulated rainfall of the event; RI_{MAX}: maximum rainfall intensity; API: antecedent precipitation index; Q_{MAX}: peak discharge during the flood event; Q_{TOT}: total volume of stream water exported during the event; Q_{OF-TOT}: total volume of surface runoff exported during the event; Q_{OF-TOT}%: percentage of surface runoff during the event calculated as $Q_{OF-TOT}/Q_{TOT}*100$; K_E: flow coefficient calculated as Q_{TOT}/R_{TOT}; n: sample size; $[TSS]_{mean}$: flood-event mean total suspended sediments concentration; $Turbidity_{mean}$: flood-event mean turbidity; $[E.\ coli]_{mean}$: flood-event mean *E. coli* concentration. Measurements of EC and of Turbidity were lacking for events A and G, respectively. Although *E. coli* measurements for events C-E were expressed in CFU 100 mL^{-1}, they are reported as MPN 100 mL^{-1} for the sake of simplicity.